

RESEARCH ARTICLE

10.1002/2013JD020934

Key Points:

- First estimates of hurricane intensity using GPS
- Hurricanes' eyewall vertical thermal structure observed with GPS
- GPS shows promise in augmenting current hurricane data sets

Correspondence to:

P. Vergados,
Panagiotis.Vergados@jpl.nasa.gov

Citation:

Vergados, P., Z. J. Luo, K. Emanuel, and A. J. Mannucci (2014), Observational tests of hurricane intensity estimations using GPS radio occultations, *J. Geophys. Res. Atmos.*, 119, 1936–1948, doi:10.1002/2013JD020934.

Received 23 SEP 2013

Accepted 16 JAN 2014

Accepted article online 20 JAN 2014

Published online 25 FEB 2014

Observational tests of hurricane intensity estimations using GPS radio occultations

Panagiotis Vergados¹, Zhengzhao Johnny Luo², Kerry Emanuel³, and Anthony J. Mannucci¹¹NASA Jet Propulsion Laboratory, California Institute of Technology, Pasadena, California, USA, ²Department of Earth and Atmospheric Science and CREST Institute, City College of New York, New York, New York, USA, ³Program in Atmospheres, Oceans, and Climate, Massachusetts Institute of Technology, Cambridge, Massachusetts, USA

Abstract This study presents a novel approach to estimating the intensity of hurricanes using temperature profiles from Global Positioning System radio occultation (GPSRO) measurements. Previous research has shown that the temperature difference between the ocean surface and the eyewall outflow region defines hurricanes' thermodynamic efficiency, which is directly proportional to the storm's intensity. Outflow temperatures in the eyewall region of 27 hurricanes in 2004–2011 were obtained from GPSRO observations. These observations, along with ocean surface temperatures from NASA Modern Era-Retrospective Analysis for Research and Applications, made it possible to estimate hurricane intensities using a simplified hurricane model. Our preliminary results are quantitatively consistent with best-track values from the National Hurricane Center within 9.4%. As a by-product of our study, we present for the first time GPSRO vertical temperature profiles in the vicinity of the eyewall region of hurricanes, which we compared with collocated temperature profiles from the European Centre for Medium-Range Weather Forecasts Reanalysis Interim (ERA-Interim). Some of the GPSRO data sets reveal a double tropopause in the vicinity of the eyewall—a characteristic that we do not see in ERA-Interim. We conclude that GPSRO observations can be of supplementary assistance in augmenting existing data sets used in hurricane intensity estimation. GPSROs' cloud-penetrating capability and high vertical resolution can be useful in providing soundings in the area close to the eyewall region of hurricanes revealing detailed information about their thermal structure, potentially advancing our current knowledge of their dynamics, evolution, and physics.

1. Introduction

Hurricanes are potent natural hazards with high socioeconomic impacts [Murnane and Elsner, 2012]. Their power dissipation has increased over the years [Emanuel, 2005] as the intensity of strong hurricanes strengthens [Elsner et al., 2008]. Yet little progress has been made in hurricane intensity predictions compared to track forecasting [e.g., Harnos and Nesbitt, 2011, and references therein]. DeMaria et al. [2013] report that although hurricane intensity forecasts improve every year, their rate of improvement is still slower than that of their track forecasts based on a study over the past 24 years. This is partly due to limited knowledge of their current intensity and physics [Kaplan and DeMaria, 2003].

Hurricane intensity is commonly measured by the storm's maximum sustained wind (MSW), defined as the 1 min average wind speed at the altitude of 10 m at the National Hurricane Center (NHC). Although in situ measurements of MSW are possible through reconnaissance aircraft or land/ship-based instruments, satellites have been the major source of information due to their global availability. The Dvorak technique is the primary satellite method for estimating MSW based on cloud pattern recognition from visible and infrared (IR) images [Dvorak, 1975; Veldon et al., 2006 for a review]. There are also other methods such as one that relates the warm anomaly of the microwave oxygen band brightness temperature (~55 GHz) to the hurricane pressure gradient [Kidder et al., 1978].

Recently, Wong and Emanuel [2007] proposed a new method to estimate hurricane intensity based on modeling a hurricane as a balanced convectively neutral vortex. Luo et al. [2008] tested that method using data from CloudSat and Moderate Resolution Imaging Spectroradiometer, showing promising results. Here we extend the Wong and Emanuel [2007] method using observations from the Global Positioning System (GPS).

Briefly, Global Positioning System radio occultation (GPSRO) is a limb-viewing technique that requires a GPS and a Low Earth Orbiter (LEO) located on opposite sides of the Earth's limb [Kursinski et al., 1997] (cf., Figure 1). The GPS satellite transmits dual-frequency radio wave signals (~1.2 GHz and ~1.5 GHz), whose amplitude and

Tropical cyclone cross-section & GPS radio occultation geometry

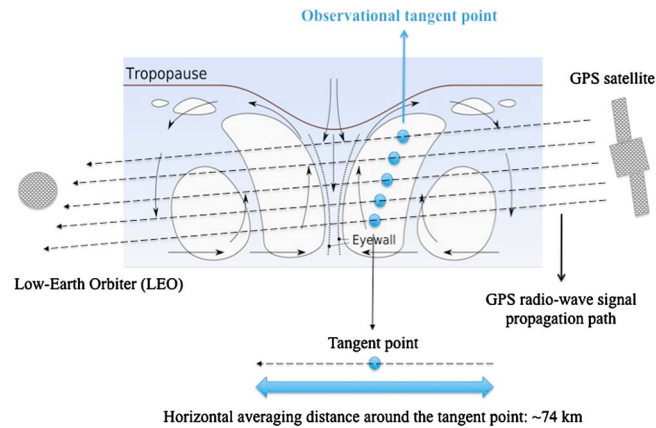


Figure 1. Simplified schematic of GPS radio wave signals traversing the eyewall of a tropical cyclone. The dashed black lines show the GPS radio wave signal propagation paths, and the blue dots correspond to the GPS radio occultation observation tangent points. The GPS radio occultation observation at the tangent point represents the mean state of the atmosphere that is averaged over the horizontal distance along the signal propagation as shown at the bottom of the schematic, with the majority of the information coming from the tangent point.

phase are recorded by a GPS antenna onboard LEOs as a function of occultation time. From the recorded phase measurements, we subtract the phase of the GPS signals that would have been measured in the absence of the Earth’s atmosphere. The resulting phase is termed excess phase delay; from which the Doppler shift of the GPS signals as a function of occultation time is estimated.

The Doppler shift estimates are then used to compute the amount of bending of the GPSRO signals, which is then used to compute the refractive index of the atmosphere at the tangent point of the occultation [Hajj et al., 2002, and references therein]. The relative movement of the GPS-LEO satellite pair allows for the vertical scanning of the Earth’s atmosphere and thus of the retrieval of vertical profiles of atmospheric refractivity with a vertical resolution of 100–200 m in the troposphere [Fjeldbo et al., 1971]. Microwave theory states that the atmospheric refractive index is directly proportional to the atmospheric temperature, pressure, and water vapor [Papas, 1965]:

$$N = (n - 1) \cdot 10^6 = 77.6 \frac{P}{T} + 3.73 \cdot 10^5 \frac{e}{T^2} \tag{1}$$

where n (unitless) is the atmospheric refractive index, N (unitless) the atmospheric refractivity, P (in mbar) the total atmospheric pressure, T (in K) the atmospheric temperature, and e (in mbar) the water vapor pressure. Both the dry term (first term at the right-hand side (RHS) of equation (1)) and the wet term (second term at the RHS of equation (1)) contribute to the atmospheric refractivity, and thus, independent temperature (water vapor pressure) information must be provided in order to retrieve water vapor pressure (temperature) profiles. Healy and Eyre [2000] describe in detail the one-dimensional variational assimilation (1D-Var) technique applied to retrieve both temperature and water vapor profiles from vertical profiles of atmospheric refractivity.

GPS has emerged as a complementary remote-sensing instrument that provides unprecedented measurements of the thermodynamic environment inside and around the thick clouds and heavy precipitation of hurricanes [Vergados et al., 2013]—regions in which visible, IR, and microwave (MW) satellite measurements are largely contaminated. Biondi et al. [2011] studied the GPSRO bending angle and temperature anomalies in the upper troposphere/lower stratosphere (UT/LS) during hurricanes using the 1D-Var-based products provided by the Constellation Observing System for Meteorology, Ionosphere and Climate (COSMIC) [Anthes et al., 2008] Data Analysis and Archive Center (CDAAC).

Liu et al. [2012] assimilated GPSRO observations in an ensemble filter assimilation system, demonstrating improvements both in the initial vortex formation and storm intensification. Biondi et al. [2013] identified clear signatures of hurricane cloud top heights in bending angle and temperature profiles using GPS radio occultation (GPSRO) observations. Vergados et al. [2013] demonstrated through a composite analysis of 42 hurricanes that GPSRO data sets can capture the moist thermodynamic structure of hurricanes and their

morphological characteristics. Evidently, GPSRO data sets have the potential to augment and complement current research to improve the diagnosis and prediction of hurricanes.

The National Aeronautics and Space Administration (NASA) also invests considerably in hurricane intensity forecasting through the Cyclone Global Navigation Satellite System (CYGNSS) mission, highlighting the importance of GPS technology in advancing our current understanding of various hurricane intensification processes and their role in modulating hurricane intensity. CYGNSS is designed to study key air-sea interaction processes near the inner core of rapidly changing storms [Ruf *et al.*, 2012] by analyzing reflected GPS radio wave signals from the ocean surface, from which sea surface wind velocities can be inferred.

Accomplishing any goal related to improving hurricane intensity forecasting requires integration of existing observational data sets and models. In this study, our overarching goals are (a) to stress the importance, in terms of information content, of the suitability of the GPSRO observations for estimating hurricane intensities using the Wong and Emanuel [2007] technique and (b) to provide additional tests of the feasibility of the Wong and Emanuel [2007] simplified model in estimating hurricane intensities. We present a coordinated effort that integrates a hurricane model, GPSRO measurements, and NASA's Modern Era-Retrospective Analysis for Research and Applications (MERRA) data sets [Rienecker *et al.*, 2011] to directly address this research's goals.

To achieve these objectives, we perform a case study that includes 27 hurricanes in the Atlantic and the Pacific Ocean Basins, and we document and report the statistical differences and trends between our results and the 6-hourly "best-track" values obtained using the Automated Tropical Cyclone Forecasting (ATCF) system [Sampson and Schrader, 2000] at the National Hurricane Center (NHC) [Landsea and Franklin, 2013a]. Our preliminary results demonstrate that GPSRO measurements show promise in estimating hurricane intensities, which could augment current hurricane observations by introducing a new space-based data set that offers low sensitivity to clouds and heavy precipitation. This suggests that GPSRO data sets have the potential to improve hurricane intensity estimation.

It should be noted that the NHC database provides hurricane intensity values every 6 h, which are reported to the nearest 5 kt interval (1 kt = 0.514 m/s). This database is not entirely based on in situ hurricane intensity measurements, and thus, it does not represent "ground truth" estimates. However, Landsea and Franklin [2013a] present a comprehensive uncertainty analysis of all hurricane variables reported by NHC, which we can use as a guide to bind the NHC hurricane intensity values. At this moment, the NHC is the best available alternative we can use for the purpose of our study. When a much larger GPSRO hurricane database becomes available (e.g., when the Constellation Observing System for Meteorology, Ionosphere and Climate-II (COSMIC-2/FORMOSAT-7) is launched in 2016 providing $\times 10$ more GPSROs in the tropics compared to the current COSMIC-I data set), we will be able to use reconnaissance and other in situ databases for further evaluation.

Our methodology is described in section 2, while section 3 presents our initial hurricane MSW using GPSRO observations, as well as the error analysis of our results. Section 4 presents our concluding remarks.

2. Methodology

2.1. Simplified Hurricane Intensity Theory

For the purpose of this study, we use the Wong and Emanuel [2007] simplified theory, which predicts that a hurricane's maximum gradient wind speed (V_m , m/s) is proportional to (a) the difference between the sea surface temperature (SST) (T_s , K) and the outflow temperature (T_o , K) inside the eyewall and (b) the boundary layer moist static energy (MSE) difference between the eyewall (h_{eyewall} , J/kg) and the unperturbed environment (h_o , J/kg). Equations (2) and (3) show the analytical expressions for the maximum gradient wind speed and the MSE, respectively [also see Luo *et al.*, 2008, equation (1)]:

$$V_m^2 = \frac{C_K}{C_D} \left(\frac{T_s - T_o}{T_o} \right) (h_{\text{eyewall}} - h_o), \quad (2)$$

with

$$h = c_p T + gz + L_v q, \quad (3)$$

where C_K is the nondimensional surface enthalpy exchange coefficient, C_D is the drag coefficient, c_p is the dry air specific heat capacity (J/kg/K), g is the gravitational acceleration (m/s^2), L_v is the latent heat of vaporization

(J/kg), q is the specific humidity (g/kg), z is the altitude (m), and T is the temperature (K) (either at the outflow height when estimating the h_{eyewall} or at the boundary layer when estimating h_o). Because MSE is approximately conserved inside the eyewall, h_{eyewall} can be estimated from near cloud top or outflow. At the outflow height the specific humidity is small, and its contribution to the MSE is negligible, so it will not be considered in our calculations.

2.2. GPSRO Data Sets

We employ temperature profiles, from the Challenging Minisatellite Payload and COSMIC RO missions, as a function of altitude in the 2004–2011 period provided by CDAAC (cf., <http://cdaac-www.cosmic.ucar.edu/cdaac/research.html>). Specifically, we use the “wetPrf” data files in which the temperature profiles are given in a 100 m vertical resolution and an accuracy of about 0.2–0.5 K [Hajj *et al.*, 2004].

2.2.1. GPSRO Horizontal Footprint

GPSRO observations are limb-viewing measurements. The temperature at each altitude corresponds to the mean-weighted temperature averaged over a horizontal distance along the GPS signal propagation path. Theoretically, excluding ionospheric error noise or horizontal inhomogeneities, this horizontal distance is a function of the instrument’s vertical resolution: $\Delta H = 2\sqrt{2R\Delta Z}$ [Kursinski *et al.*, 1997], where R is the local curvature of the Earth’s atmosphere at the tangent point and ΔZ is the vertical resolution. Typically, the vertical resolution is a function of the retrieval process (geometric optics or wave optics) of the GPSRO profiles, and in general, it ranges between 0.5 km and 1.4 km between the lower troposphere and middle atmosphere.

However, the wave optics retrieval yields profiles with significantly better vertical resolution than the geometric optics retrieval, and in this study, the CDAAC temperature profiles are provided with a 100 m vertical resolution. In our case, and in ideal conditions, a vertical resolution of 100 m at 15 km altitude translates to a horizontal averaging of < 100 km. Given that the GPSRO weighting functions peak at the tangent point during an occultation [Kursinski *et al.*, 2000], we are confident that the majority of the atmospheric information represents the state of the atmosphere at the tangent point (cf., Figure 1). We must mention that there will be a smearing effect due to the horizontal averaging, and thus, the GPSRO temperatures at the tangent point will contain contributions from the surrounding environment.

2.2.2. Eyewall Dimension

Liu *et al.* [1999] estimated an eyewall width of 60 km based on model simulations. Cecil *et al.* [2002] studied 45 hurricanes using data from the Tropical Rainfall Measuring Mission, estimating a median eyewall width of 50 km. Teshiba *et al.* [2005] reported the formation of a circular eyewall near the Naze radar site of 50 km radius using rawinsonde observations. Rozoff *et al.* [2008] reported eyewall widths of 50 km based on aircraft observations over hurricane Frances. Yang *et al.* [2013] found eyewall widths larger than 60–70 km based on passive microwave satellite imagery of hurricanes in the western North Pacific Basin from 1997 to 2011 period. Thus, we adopt an eyewall width of 50 km.

2.2.3. GPSRO—Eyewall Collocation

We use the NHC database to identify the track forecasting (latitude and longitude) of the center of each hurricane during its lifetime. Because the Wong and Emanuel [2007] hurricane model requires only the temperature at the outflow height, we use the geographic coordinates of the tangent points around the tropopause to calculate the distance the GPSRO occurred from the center. Given the radius of maximum winds in the NHC data files (that defines the inner radius of a hurricane’s eyewall) and assuming an average eyewall width of 50 km, we can collocate the GPSRO with respect to the eyewall region. In this preliminary study, we enforced a temporal separation window of less than 30 min between the time of the GPSRO sounding and of the passage of the hurricane center, and we found 27 cases.

However, we must point out that even if we collocate the tangent point of each GPSRO with the eyewall region, the GPSRO horizontal footprint (discussed in section 2.2.1) is comparable with the dimension of the eyewall. Taking that into account and the fact that a hurricane is a fast-developing system, our GPSRO events could fall in the surrounding area of the hurricanes’ eyewall, providing an average thermal structure of the eyewall and its vicinity. Thus, this point forth, we refer to GPSRO collocations with respect to the vicinity of the eyewall region.

Also, looser temporal criteria could have been used. This is because even during a hurricane’s fast development, knowing its wind speed, the time the GPSRO occurred, and the hurricane’s spatiotemporal

information, one can evaluate whether a GPSRO sounding occurred in the vicinity of the eyewall region. The results presented herein are representative of the hurricane data set in the time period 2004–2011, which itself is a subset of the entire hurricane record. Expanding the current study period and given that COSMIC-2/FORMOSAT-7 will provide $\times 10$ more RO soundings, we are confident that our sampling size will increase.

2.2.4. Eyewall Outflow Temperature and Moist Static Energy

As an air parcel ascends beyond its level of neutral buoyancy, it continues rising at the dry adiabatic lapse rate while the environment cools at a smaller rate. Hence, boundary layer air overshoots inside the eyewall and will be colder than the ambient tropopause. For this reason, and to keep the calculations simple, we approximate the coldest temperature and the altitude where it occurs as the outflow temperature, T_o , and the outflow height, z , in the right-hand side (RHS) of equation (2), as well as in equation (3) to estimate the eyewall MSE, which we substitute into the term called h_{eyewall} in the RHS of equation (2).

This procedure should result in an accurate estimate of eyewall MSE but risks an underestimate of T_o . We assume that the eyewall is saturated, so that the MSE is a function only of temperature and altitude. We can do this, because the MSE is approximately constant with altitude, due to the convective neutrality of the moist troposphere. We quantitatively characterize the error in hurricane intensity estimation due to the uncertainty in the outflow temperature and in the MSE by performing an error analysis shown in section 3.3. Previous researchers have approximated the outflow height as the tropopause height [Emanuel and Rotunno, 2011; Emanuel et al., 2013].

2.3. Eyewall Sea Surface Temperature

Given the hurricane location, we use the Modern Era-Retrospective Analysis for Research and Applications (MERRA) to estimate the SST in the eyewall region, the term called T_s in the RHS of equation (2). Given the width of the eyewall and provided that the horizontal temperature gradients inside the eyewall are small, then MERRA, having a horizontal resolution of $0.75^\circ \times 0.5^\circ$, provides an accurate eyewall SST. Although these are very good assumptions to obtain the average SST of the eyewall, MERRA's horizontal resolution cannot capture smaller-scale horizontal temperature gradients that may occur across the eyewall. Therefore, in our error analysis we also account for hurricane intensity errors due to errors in the eyewall SST.

2.4. Moist Static Energy of the Unperturbed Environment

We define the unperturbed environment to be located at a distance equal to the radius of the outermost closed isobar (ROCI), whose value is also provided for each hurricane throughout its lifetime by ATCF at NHC. Knowing the location of the eye and ROCI of each storm, we use MERRA to estimate the MSE of the boundary layer of the unperturbed environment, the term called h_o in the RHS of equation (2). Again, MERRA is an analysis given in a specified grid; thus, the temperature of the unperturbed environment may also contain errors, which we take into account when estimating the hurricane intensity error in section 3.3.

2.5. Estimating Hurricane Intensity

Given the relatively narrow eyewall area and the fact that GPSRO observations are randomly occurring around the globe, although we managed to obtain ~ 4500 GPSRO profiles for the North Atlantic and Western Pacific hurricanes in the period 2004–2011, only 27 profiles fell in the vicinity of the eyewall region (cf., Tables 1 and 2). The 4500 profiles are a composite of 42 hurricanes. We selected them, allowing a 600 km spatial window from the storms' center to cover the largest hurricanes and a temporal window of 30 min. This small number of case studies resulted from the combination of the stringent criteria we used to obtain the GPSRO temperature profiles in the eyewall region, as well as the limited time period we studied.

At this preliminary stage of our research, we considered most appropriate to first test, and demonstrate, the efficacy of GPSRO measurements in estimating hurricane intensities. Owing to the randomness of the GPSRO soundings, the COSMIC profiles correspond to random temporal moments of the hurricane's lifetime; thus, we estimate the hurricanes' intensity at a given time during its lifetime. Along with the intensity estimates, we also report the date when the estimate occurred to compare with the NHC.

Table 1. Temperature and Moist Static Energy Values of the Eyewall and the Unperturbed Environment

TC Name	Date	$T_{outflow}$ (K)	$T_{surface}$ (K)	MSE _{eyewall} (J/Kg)	MSE _{environ.} (J/Kg)
Chantal	31/07/2007	207.4	299.1	343,677	336,603
Merbok	07/08/2011	195.3	300.0	351,117	343,000
Edouard	05/08/2008	205.2	302.1	346,366	341,920
Dolphin	15/12/2008	189.8	302.1	360,289	349,548
Dennis	09/07/2005	196.0	302.3	360,640	349,507
Bill	17/08/2009	194.6	300.2	352,533	346,345
Bertha	08/07/2008	197.4	300.2	354,524	343,095
Jangmi	28/09/2008	193.2	295.3	371,546	360,669
Neoguri	18/04/2008	190.9	299.0	358,455	344,993
Melor	03/10/2009	190.4	302.2	361,872	341,631
Bill	20/08/2009	195.2	301.6	359,275	341,367
Sepat	18/08/2007	193.2	297.8	361,125	350,253
Vamco	21/08/2009	197.9	301.7	363,000	347,976
Sepat	16/08/2007	194.6	302.8	371,172	337,957
Tomas	30/10/2010	191.4	302.0	352,220	344,031
Paula	12/10/2010	189.5	302.5	354,275	343,629
Julia (1)	14/09/2010	191.5	300.9	354,282	344,022
Julia (2)	14/09/2010	196.6	300.6	348,617	342,123
Igor	15/09/2010	190.3	301.9	358,021	343,807
Ida	08/11/2009	195.08	301.8	350,072	340,374
Helene	17/09/2006	191.7	300.7	352,521	342,942
Frances	04/09/2004	193.3	302.0	358,063	345,359
Dolly	21/07/2008	193.5	301.6	346,543	342,651
Dean	18/08/2007	196.3	302.0	373,821	345,536
Bill	18/08/2009	194.9	300.3	358,721	341,432
Bill	18/08/2009	192.1	300.2	356,897	341,281
Bertha	04/07/2008	195.4	300.1	359,203	339,529

For these 27 case studies, we recorded the outflow temperature and the SST, and we calculated the MSE of the eyewall and of the unperturbed environment. Then, we substituted these values into the RHS of equation (2) to estimate the intensity of the 27 hurricanes using the COSMIC and MERRA data sets. Tables 1 and 2 show the results. Then, we compared our results against the NHC followed by an error sensitivity analysis due to temperature errors.

Table 2. Hurricane Wind Speeds Estimated From GPSRO and as Provided by the NHC

TC Name	Date	NHC wind (m/s)	GPSRO wind (20% adjust, m/s)	GPSRO wind (10% adjust, m/s)
Chantal	31/07/2007	23	32	36
Merbok	07/08/2011	36	37	42
Edouard	05/08/2008	28	26	29
Dolphin	15/12/2008	41	45	51
Dennis	09/07/2005	39	44	49
Bill	17/08/2009	38	33	37
Bertha	08/07/2008	46	44	49
Jangmi	28/09/2008	44	43	48
Neoguri	18/04/2008	46	49	56
Melor	03/10/2009	59	62	69
Bill	20/08/2009	57	56	63
Sepat	18/08/2007	51	44	49
Vamco	21/08/2009	59	50	57
Sepat	16/08/2007	71	77	86
Tomas	30/10/2010	43	39	44
Paula	12/10/2010	46	45	50
Julia (1)	14/09/2010	41	43	49
Julia (2)	14/09/2010	31	33	37
Igor	15/09/2010	59	52	59
Ida	08/11/2009	44	41	46
Helene	17/09/2006	36	41	47
Frances	04/09/2004	44	48	54
Dolly	21/07/2008	23	26	30
Dean	18/08/2007	64	69	78
Bill	18/08/2009	49	53	60
Bill	18/08/2009	47	52	59
Bertha	04/07/2008	54	58	66

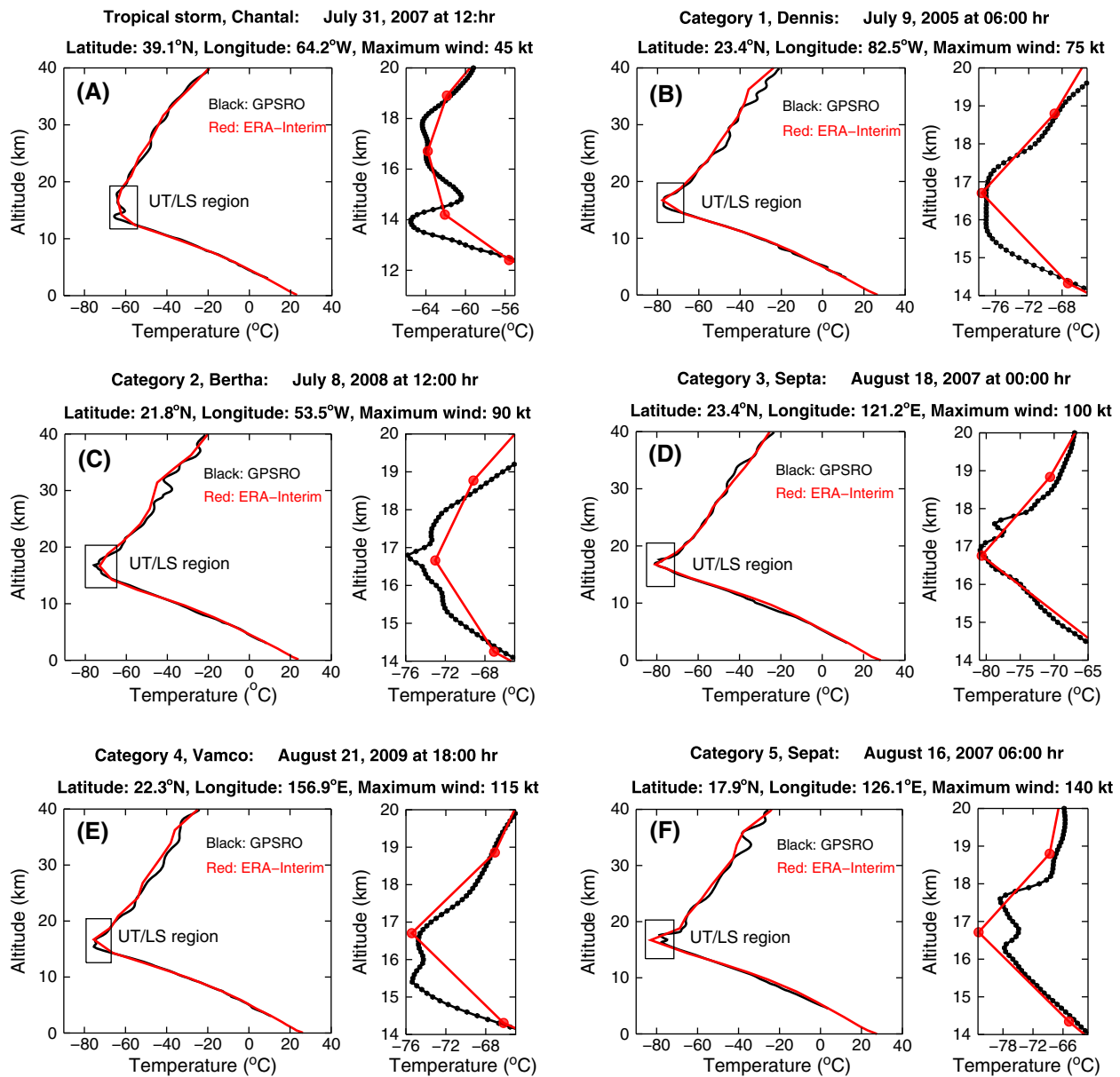


Figure 2. (a–f) Vertical temperature profiles inside the eyewall of six tropical cyclones, enlarging the upper troposphere/lower stratosphere region and emphasizing the outflow area. In all graphs, the black lines indicate the GPSRO profiles and the red lines represent the collocated ERA-Interim profiles.

3. Results

3.1. Eyewall Thermal Structure

In the tropics, air enters the upper troposphere predominantly via deep convection [Riehl and Malkus 1958; Riehl and Simpson 1979], which under extreme conditions introduces detrained air into the upper troposphere/lower stratosphere (UT/LS) region. Hurricane eyewalls favor such large-scale vertical updrafts that can lead to convective overshoots to stratospheric altitudes [e.g., Romps and Kuang, 2009].

Figure 2 shows the vertical thermal structure in the eyewall region of six hurricanes observed from GPSRO (black) and the European Centre for Medium-Range Weather Forecasts Reanalysis Interim (ERA-Interim) (red) data sets, and we mark the UT/LS layer with black rectangles shown at the RHS of each graph. In the six examples of GPSRO (black) vertical temperature profiles, we observe that some cases display a double tropopause (cf., Figures 2a, 2d, 2e, and 2f) possibly due to deep convection, but some other cases only show a

local temperature minimum (cf., Figures 2b and 2c). The double tropopause captured by the GPSRO data (black) is not captured by ERA-Interim (red).

We must clarify here that the double tropopause is not necessarily a characteristic of the eyewall region but in general of regions characterized by convective cloud activity [Danielsen, 1993; Chaboureau *et al.*, 2007; Biondi *et al.*, 2012, 2013]. Although such a phenomenon is not completely understood, it has been hypothesized that a possible reason is the superposition of layers of air from two different sources [Danielsen, 1982; Reid and Gage, 1996]. In the case of hurricanes, Simpson *et al.* [1998], Montgomery *et al.* [2006], and Molinari and Vollaro [2008] theorized that convective bursts inside the eyewall overshoot air from the boundary layer into the UT/LS region, which overlay on the ambient tropopause, forming a double tropopause.

Another characteristic signature is that the tropopause layer is higher in stronger hurricanes (~17.8 km in Cat-5) than in weaker storms (~13.9 km in tropical storms), a behavior also reported by Koteswaram [1967]. This is characteristic of all cases we examined, not shown here due to limited space. A possible explanation for this is that stronger hurricanes have more organized structure and stronger cores and are characterized by deeper convection than the amorphous and weaker storms; thus, the level of neutral buoyancy for deep convection is higher. Unlike the high vertical resolution GPSRO measurements, the ERA-Interim profiles neither capture a double tropopause nor display a gradual upward displacement of the tropopause altitude with increasing hurricane intensity.

3.2. Maximum Wind Speed

Potential intensity theory shows that the square of the gradient wind varies as a function of the ratio, C_K/C_D , of the surface enthalpy exchange coefficient to the surface drag coefficient [Emanuel, 2004]. Yet we have little knowledge of the value of these coefficients in hurricanes.

3.2.1. C_K/C_D Ratio

DeCosmo *et al.* [1996] reported an average value of ~0.5 for the C_K/C_D ratio for hurricanes with wind speeds between 50 and 72 m/s based on measurements from the Humidity Exchange over the Sea program. Zhang *et al.* [2008] showed that for hurricane wind speeds up to 30 m/s, the C_K/C_D ratio assumes a mean value of 0.63, based on observations from the Coupled Boundary Layers Air-Sea Transfer (CBLAST) field program.

Haus *et al.* [2010] using laboratory experiments reported that the C_K/C_D ratio obtains an almost constant value of ~0.5 for hurricanes with wind speeds between 30 and 40 m/s. Bell *et al.* [2012] estimated that C_K/C_D obtains a mean value of 0.48 based on CBLAST results in hurricanes Fabian and Isabel. Here we will also assume a value of 0.5 for the C_K/C_D ratio, which is both a realistic and consistent assumption based on field campaigns and laboratory experiments, and it suffices for the purpose of our study.

3.2.2. Adjustment to 10 m Level Wind Speed

The Wong and Emanuel [2007] gradient wind speed model is valid near the top of the boundary layer [Luo *et al.*, 2008]. Thus, we must adjust our estimates to the 10 m level to directly compare them with the NHC best-track data values. The adjustment factor depends on the air-sea temperature difference and the sea surface roughness [Thompson and Cardone, 1996].

Powell *et al.* [1996] suggested a 20% adjustment of the boundary layer winds, and Russell [1971], Batts *et al.* [1980], Georgiou *et al.* [1983], and Vickery and Twisdale [1995] defined the ratio of the surface level winds to the gradient level winds to be 0.8–0.9. Vickery *et al.* [2000] adopted a 10% difference between the boundary layer winds and surface winds in the eyewall region in their model, while Franklin *et al.* [2003, Table 2], using GPS dropwindsonde profiles, found that the surface level wind to the upper level wind ratio should be ~0.9 in the eyewall area, but they also reported greater values.

NHC empirically adjusts the boundary layer winds, at the eyewall, by 10% to estimate the surface winds [Franklin, 2013]. Therefore, in our study we will present two different data sets: one with a 10% adjustment and another one with a 20% adjustment.

3.2.3. Results

We compared our estimates of the hurricane intensity with those from the NHC (cf., Figure 3a), and we performed an error analysis of the GPSRO-estimated hurricane intensity owing to temperature errors. We used the GPSRO temperatures to constrain and quantify the hurricane intensity uncertainties arising from our assumptions (cf., section 3.3).

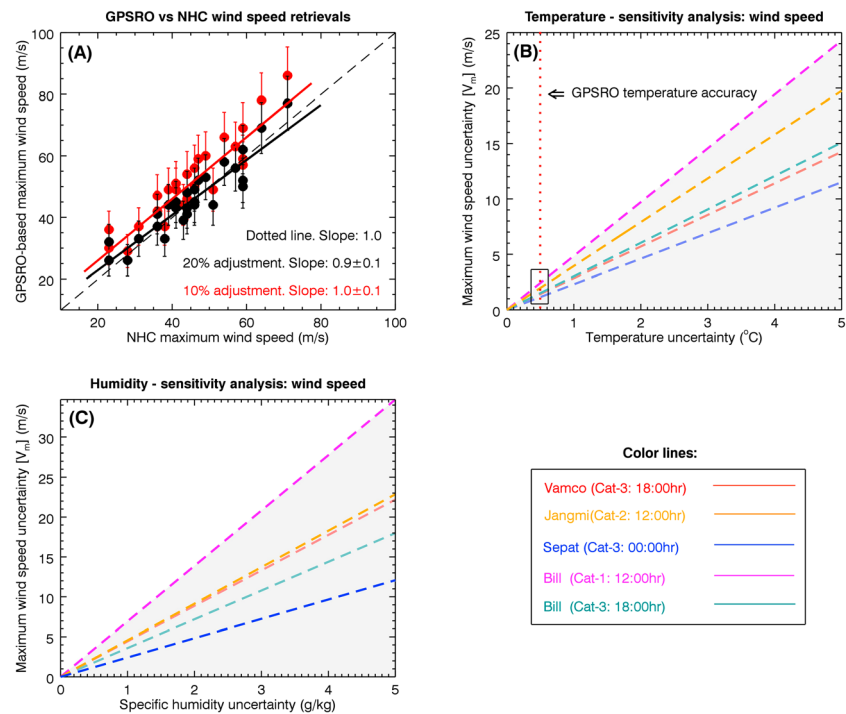


Figure 3. (a) GPSRO-based maximum wind speed values are compared with the National Hurricane Center best-track data values. Solid circles represent the GPSRO-NHC wind speed pairs when 10% (red) and 20% (black) reduction is applied to the GPSRO values, and the solid lines represent their linear regression. The dotted line shows the slope 1.0 line. (b) Maximum gradient wind speed uncertainty in response to plausible temperature errors for hurricanes Vamco (red), Sepat (blue), Bill (teal), Jangmi (orange), and Bill (magenta). The red dotted line represents the GPSRO temperature accuracy. The black rectangle indicates the maximum wind speed error corresponding to the GPSRO temperature uncertainty level. (c) Maximum gradient wind speed uncertainty in response to specific humidity errors.

Figure 3a shows the GPSRO-NHC pairs (black circles) and their respective error bars, after applying a 20% adjustment on the GPSRO-based estimates. The GPSRO-based wind error bars are computed as the standard deviation of the GPSRO-based wind estimates. The solid black line shows the linear regression fit to the pair of data with a slope of 0.9 ± 0.1 and a y intercept of 5.1 ± 4.8 , which are statistically significant to the 95% confidence level based on the Student's *t* test statistics. The mean absolute error and root-mean-square error (RMSE) between the GPSRO-derived and NHC hurricane intensity estimates, for all 27 profiles employed in this study, are 4.0 m/s and 4.5 m/s, respectively. For reference, we also show the dotted black line with a slope of 1.

We also present GPSRO-derived hurricane wind values reduced by 10% (cf., Figure 3a; red circles), and the linear regression model showed a slope of 1.0 ± 0.1 and a y intercept of 6.0 ± 5.1 , which are statistically significant to the 95% confidence level. Again, the mean absolute error and RMSE of the GPSRO-NHC pairs, for all 27 case studies, are 7.0 m/s and 8.3 m/s, respectively. We observe that a 20% adjustment of the GPSRO-derived intensities produces much smaller biases and RMSE than that of the 10% adjustment. Also, a probable explanation of the nearly constant offset between the GPSRO-derived hurricane intensities and the NHC values might be the fact that the offset between the measured and true outflow temperature is approximately constant across all cases.

The results indicate that GPSRO temperature profiles can be used to estimate hurricane intensity with useful accuracy and precision. Table 1 shows the name, the date, the outflow temperature in vicinity of the eyewall region, the SST, and the MSEs of the eyewall and the unperturbed environment. Table 2 shows the altitude of the coldest point in the eyewall region, the GPSRO-based wind speed estimates, and the NHC wind speed estimates. We observe that the eyewall MSE at the outflow is systematically higher than the MSE of the boundary layer of the unperturbed environment.

3.3. Error Analysis

The GPSRO-based estimated intensities are subject to errors in the temperature of the outflow in the eyewall (T_o), of the unperturbed environment (T'_o), and of the sea surface (T_s). The error sources for each of these

temperatures are different; however, for the sensitivity test, we will assume that the magnitude of all temperature errors is the same ($\sigma_T = \delta T_s = \delta T_o = \delta T'_o$, K). Differentiating equation (1) with respect to T_o , T_s , and T'_o , we obtain an expression that gives the hurricane intensity error (σ_{V_m} , m/s), due to temperature error:

$$\begin{aligned}
 (\sigma_{V_m})^2_T &= \left(\frac{\partial V_m}{\partial T_o}\right)^2 \delta T_o^2 + \left(\frac{\partial V_m}{\partial T_s}\right)^2 \delta T_s^2 + \left(\frac{\partial V_m}{\partial T'_o}\right)^2 \delta T_o^2 \stackrel{\delta T_o = \delta T_s = \delta T'_o = \sigma_T}{\Leftrightarrow} \\
 (\sigma_{V_m})_T &= \frac{1}{2V_m} \frac{C_K}{C_D} \frac{1}{T_o} \sqrt{\Delta h^2 + [c_p(T_s - T_o)]^2 + \left[c_p(T_s - T_o) - \frac{T_s}{T_o} \Delta h\right]^2} \cdot \sigma_T \quad (4)
 \end{aligned}$$

Figure 3b shows that the intensity error increases linearly as a function of temperature uncertainty. The stronger the hurricane, the smaller the intensity error, implying that the *Wong and Emanuel* [2007] hurricane simplified model works better for stronger hurricanes—a result similar to that found in *Luo et al.* [2008]. Although the GPSRO and MERRA temperature profiles are accurate to 0.5 K and 0.5–1.0 K [*Rienecker et al.*, 2011], respectively, we show temperature errors up to 5.0 K. It is shown that a 0.5 K temperature error (black rectangle) in GPSRO and MERRA profiles introduces an average of ~1–3 m/s error in intensity estimation, which increases to ~5–12 m/s at 2.5 K temperature error (depending on the tropical cyclone (TC) intensity), reaching 11–24 m/s at 5.0 K temperature error. We also examined the sensitivity of our technique to specific humidity uncertainty from MERRA (cf., Figure 3c). Taking again the partial derivative of the maximum wind speed as a function of specific humidity, we obtain

$$(\sigma_{V_m})^2_q = \left(\frac{\partial V_m}{\partial q}\right)^2 \sigma_q^2 \Leftrightarrow (\sigma_{V_m})_q = \frac{L_v V_m}{2 \Delta h} \sigma_q \quad (5)$$

Figure 3c shows that a 1.0 g/kg (or 5.0%) specific humidity error introduces 2–7 m/s intensity error that increases linearly to 12 m/s for Category 3 hurricanes and 34 m/s for Category 1 hurricanes given a 5.0 g/kg specific humidity error. *Landsea and Franklin* [2013a] report that the NHC provides hurricane intensity estimates with an average uncertainty of ~5.0 m/s, which is in accordance with our current intensity estimation error.

3.4. Technique Improvement

We believe that we can improve our method in three ways, reducing the uncertainty in the GPSRO-based hurricane intensity estimation.

Key to the retrieval of hurricane intensity in the *Wong and Emanuel* [2007] simplified hurricane theory is the estimation of the MSE difference between the eyewall and the unperturbed environment. Had we obtained simultaneous GPSRO temperature profiles in the eyewall region and in the unperturbed environment, we could have estimated the parameter, Δh , by simply comparing the two GPSRO temperature profiles (K. Emanuel, personal communication, 2013). Hence, we would not need MERRA measurements to calculate the environmental MSE, and thus, we would have removed from our results the sensitivity to MERRA. Provided that the current GPSRO temperature profiles have an accuracy of 0.5 K, our results would introduce an error of only 1–3 m/s in the hurricane intensity estimation.

Another key parameter in hurricane intensity estimation is the proper characterization of the outflow height inside a hurricane's eyewall. If we had collocated CALIPSO or CloudSat measurements, we would have known more precisely the cloud top heights. We could have used these altitudes to find the GPSRO temperatures corresponding to these altitudes; thus, estimating more precisely the eyewall MSE.

Additionally, uncertainties in the position of the hurricanes' center and spatiotemporal collocation of the GPSRO soundings with respect to the hurricanes' eyewall region can introduce errors in the calculation of the eyewall MSE. Specifically, *Landsea and Franklin* [2013b] report a position uncertainty of ~35 n mi (1 nautical mile = 1.852 km) for tropical storms and ~20 n mi for Categories 1 and 2 and major hurricanes using solely satellite observations. These uncertainties decrease when aircraft measurements are included in the position

estimation (e.g., the Atlantic hurricanes we study here). We refer the reader to *Landsea and Franklin* [2013b, Figure 5 and Table 2] for a detailed discussion on hurricane position uncertainty. The combined effects of the hurricane position uncertainty, the fast development of the hurricane, the narrow eyewall width, the GPSRO's horizontal footprint (~ 100 km = 54 n mi), and the limited GPSRO soundings in the vicinity of the eyewall area can lead to collocation mismatches, which in turn can introduce systematic biases in the eyewall thermal structure and its MSE estimation.

Finally, advancements on the GPSRO atmospheric parameter techniques can improve the vertical and horizontal footprints of the radio occultations observations. This will allow better measurements of the thermal structure of hurricanes' eyewall region, which in turn will improve the MSE eyewall estimation and in extent the hurricanes' intensity.

In this preliminary stage, our overarching objective is to demonstrate for the first time the usefulness of the GPSRO measurements to inferring hurricane intensity and explain the method. Our next steps are to perform further refinements in our technique to obtain better results from what is reported herein.

4. Conclusions

The main conclusions of this study are that (a) we demonstrate the feasibility of utilizing the GPSRO observations to capture the vertical thermal signatures of the UT/LS region around the vicinity of eyewall in hurricanes and (b) provide additional tests of the hurricane intensity estimates based on the *Wong and Emanuel* [2007] technique given the instruments' observational limitations. The *Wong and Emanuel* [2007] technique requires simultaneous temperature and height readings of the eyewall of the hurricanes, which are difficult to obtain from traditional passive visible, IR, and MW observations due to possible contamination by thick clouds and heavy precipitation.

The low sensitivity of GPSRO measurements to clouds and precipitation makes them an ideal tool for this study. We showed that GPSRO measurements have the potential to provide the thermal structure of the UT/LS in the vicinity of a hurricane's eyewall with high vertical resolution (100–200 m) and that these fine structures are missing in the reanalysis data. Moreover, our results showed that the relative percentage difference between the GPSRO-derived hurricane MSW and the NHC values is $\sim 9.4\%$ on average, after reducing the GPSRO-derived winds to the 10 m level altitude by applying a 20% adjustment, while it grows to $\sim 17\%$ on average after a 10% adjustment is applied.

Nevertheless, taking into account the fact that (a) *Landsea and Franklin* [2013a] reported that the NHC hurricane intensity estimates have an average uncertainty of 4.2–5.4 m/s and (b) GPSRO-derived wind uncertainty can reach 1–3 m/s at 0.5 K temperature error implies that within the error limits, the GPSRO-derived adjusted values to the 10 m level should be in a closer agreement with NHC than the statistics we report in this study.

Given that GPS has gradually emerged as an important complementary remote-sensing instrument for measuring the thermodynamical environment inside and around hurricanes where thick clouds and heavy precipitation dominate [*Vergados et al.*, 2013], our current study further expands this line of application by using GPSRO data, coupled with a simplified hurricane model, to estimate hurricane intensities. It is encouraging to see that the GPSRO-based hurricane intensity estimates are comparable to and have the similar error characteristics as the NHC database. As an independent source of data, the GPSRO observations will thus provide an additional observational constraint to hurricane intensity estimates. Furthermore, it stands to reason that GPSRO measurements can be potentially useful in improving hurricane intensity forecasting in a synergistic way, if properly assimilated into hurricane models.

We understand that the current COSMIC mission may not provide a large sample of data inside the eyewall of hurricanes; however, the upcoming COSMIC-2/FORMOSAT-7 mission in 2016 will provide 10 times more coverage as the current COSMIC mission at the tropics, while CYGNSS (the GNSS-based NASA mission to be launched in 2016) will provide direct measurements of sea surface wind speeds at the core of hurricanes. The value of the GPS technology becomes important in hurricane monitoring. We envision creating an independent GPS-based hurricane record that can be used synergistically from the hurricane research community to observationally constrain current hurricane models and other observing remote-sensing instruments with the intent to contribute in the improvement of hurricane intensity forecasting.

Acknowledgments

This research was carried out at the Jet Propulsion Laboratory, California Institute of Technology, under a contract with the National Aeronautics and Space Administration. P. Vergados acknowledges the NPP program administered by the Oak Ridge Associated Universities (ORAU) through a contract with NASA. We would like to thank the three anonymous reviewers for providing a wealth of constructive comments, which strengthened the results of our research.

References

- Anthes, R. A., et al. (2008), The COSMIC/FORMOSAT-3 Mission: Early results, *Bull. Am. Meteorol. Soc.*, *89*, 313–333, doi:10.1175/BAMS-89-3-313.
- Batts, M. E., M. R. Cordes, L. R. Russell, J. R. Shaver, and E. Simiu (1980), Hurricane wind speeds in the United States, *Rep. No. BSS-124*, Nat. Bureau of Standards, U.S. Department of Commerce, Washington, D. C.
- Bell, M. M., M. T. Montgomery, and K. A. Emanuel (2012), Air-sea enthalpy and momentum exchange at major hurricane wind speeds observed during CBLAST, *J. Atmos. Sci.*, *69*, 3197–3222, doi:10.1175/JAS-D-11-0276.1.
- Biondi, R., T. Neubert, S. Syndergaard, and J. K. Nielsen (2011), Radio occultation bending angle anomalies during tropical cyclones, *Atmos. Meas. Tech.*, *4*, 1053–1060, doi:10.5194/amtd-4-1371-2011.
- Biondi, R., W. J. Randel, S.-P. Ho, T. Neubert, and S. Syndergaard (2012), Thermal structure of intense convective clouds derived from GPS radio occultations, *Atmos. Chem. Phys.*, *12*, 5309–5318, doi:10.5194/acp-12-5309-2012.
- Biondi, R., S.-P. Ho, W. Randel, S. Syndergaard, and T. Neubert (2013), Tropical cyclone cloud-top height and vertical temperature structure detection using GPS radio occultation measurements, *J. Geophys. Res. Atmos.*, *118*, 5247–5259, doi:10.1002/jgrd.50448.
- Cecil, D. J., E. J. Zipser, and S. W. Nesbitt (2002), Reflectivity, ice scattering, and lightning characteristics of hurricane eyewalls and rainbands. Part I: Quantitative description, *Mon. Weather Rev.*, *130*, 769–784, doi:10.1175/1520-0493(2002)130<0769:RISALC>2.0.CO;2.
- Chaboureaud, J.-P., J.-P. Cammas, J. Duron, P. J. Mascart, N. M. Sitnikov, and H.-J. Voessing (2007), A numerical study of tropical cross-tropopause transport by convective overshoots, *Atmos. Chem. Phys.*, *7*, 1731–1740, doi:10.5194/acp-7-1731-2007.
- Danielsen, E. F. (1982), A dehydration mechanism for the stratosphere, *Geophys. Res. Lett.*, *9*, 605–608, doi:10.1029/GL009i006p06005.
- Danielsen, E. F. (1993), In situ evidence of rapid, vertical, irreversible transport of lower tropospheric air into the lower tropical stratosphere by convective cloud turrets and by larger-scale upwelling in tropical cyclones, *J. Geophys. Res.*, *98*, 8665–8681, doi:10.1029/92JD02954.
- DeCosmo, J., K. B. Katsaros, S. D. Smith, R. J. Anderson, W. A. Oost, K. Bumke, and H. Chadwick (1996), Air-sea exchange of water vapor and sensible heat: The humidity exchange over the sea (HEXOS) results, *J. Geophys. Res.*, *101*, 12,001–12,016, doi:10.1029/95JC03796.
- DeMaria, M., C. Sampson, J. A. Knaff, and K. D. Musgrave (2013), Is tropical cyclone intensity guidance improving?, *BAMS*, doi:10.1175/BAMS-D-1200240.1.
- Dvorak, V. F. (1975), Tropical cyclone intensity analysis and forecasting from satellite imagery, *Mon. Weather Rev.*, *103*, 420–430, doi:10.1175/1520-0493(1975)103<0420:TCIAAF>2.0.CO;2.
- Elsner, J. B., J. P. Kossin, and T. H. Jagger (2008), The increasing intensity of the strongest tropical cyclones, *Nature*, *455*, 92–95, doi:10.1038/nature07234.
- Emanuel, K. (2004), *Tropical Cyclone Energetics and Structure*, chap. 8, pp. 165–191, Cambridge Univ. Press.
- Emanuel, K. (2005), Increasing destructiveness of tropical cyclones over the past 30 years, *Nature*, *436*, 686–688, doi:10.1038/nature03906.
- Emanuel, K., and R. Rotunno (2011), Self-stratification of tropical cyclone outflow. Part I: Implications for storm structure, *J. Atmos. Sci.*, *68*, 2236–2249, doi:10.1175/JAS-D-10-05024.1.
- Emanuel, K., S. Solomon, D. Folini, S. Davis, and C. Cagnazzo (2013), Influence of tropical tropopause layer cooling on Atlantic hurricane activity, *J. Clim.*, *26*, 2288–2301, doi:10.1175/JCLI-D-12-00242.1.
- Fjeldbo, G., A. J. Kliore, and V. R. Eshleman (1971), The neutral atmosphere of Venus as studied with the Mariner V radio occultation experiments, *Astron. J.*, *76*, 123–140, doi:10.1086/111096.
- Franklin, J. L. (2013), Use of aircraft data at the National Hurricane Center, *WMO RA-IV Workshop*, Miami, FL, USA, 12–23 March 2012 (accessed 05/31/2013). [Available at http://www.nhc.noaa.gov/outreach/presentations/nhc2013_aircraftData.pdf.]
- Franklin, J. L., M. L. Black, and K. Valde (2003), GPS dropwindsonde wind profiles in hurricanes and their operational implications, *Weather Forecast.*, *18*, 32–44, doi:10.1175/1520-0434(2003)018<0032:GDWPIH>2.0.CO;2.
- Georgiou, P. N., A. G. Davenport, and B. J. Vickery (1983), Design wind speeds in regions dominated by tropical cyclones, *J. Wind Eng. Ind. Aerodynamics*, *13*(1), 139–152, doi:10.1016/0167-6105(83)90136-8.
- Hajj, G. A., E. R. Kursinski, L. J. Romans, W. I. Bertiger, and S. S. Leroy (2002), A technical description of atmospheric sounding by GPS occultation, *J. Atmos. Sol. Terr. Phys.*, *64*, 451–469, doi:10.1016/S1364-6826(01)00114-6.
- Hajj, G. A., C. O. Ao, B. A. Iijima, D. Kuang, E. R. Kursinski, A. J. Mannucci, T. K. Meehan, L. J. Romans, M. de la Torre Juarez, and T. P. Yunck (2004), CHAMP and SAC-C atmospheric occultation results and intercomparisons, *J. Geophys. Res.*, *109*, D06109, doi:10.1029/2003JD003909.
- Harnos, D. S., and S. W. Nesbitt (2011), Convective structure in rapidly intensifying tropical cyclones as depicted by passive microwave measurements, *Geophys. Res. Lett.*, *38*, L07805, doi:10.1029/2011GL047010.
- Haus, B. K., D. Jeong, M. A. Donelan, J. A. Zhang, and I. Savelyev (2010), Relative rates of sea-air heat transfer and frictional drag in very high winds, *Geophys. Res. Lett.*, *37*, L07802, doi:10.1029/2009GL042206.
- Healy, S. B., and J. R. Eyre (2000), Retrieving temperature, water vapour and surface pressure information from refractivity-index profiles derived by radio occultation: A simulation study, *Q. J. R. Meteorol. Soc.*, *126*, 1661–1683, doi:10.1002/qj.49712656606.
- Kaplan, J., and M. DeMaria (2003), Large-scale characteristics of rapidly intensifying tropical cyclones in the North Atlantic basin, *Weather Forecast.*, *18*, 1093–1108, doi:10.1175/1520-0434(2003)018<1093:LCORIT>2.0.CO;2.
- Kidder, S. Q., W. M. Gary, and T. H. Vonder Haar (1978), Estimating tropical cyclone central pressure and outer winds from satellite microwave data, *Mon. Weather Rev.*, *106*(10), 1458–1464, doi:10.1175/1520-0493(1978)106<1458:ETCCPA>2.0.CO;2.
- Koteswaram, P. (1967), On the structure of hurricanes in the upper troposphere and lower stratosphere, *Mon. Weather Rev.*, *95*(8), 541–564, doi:10.1175/1520-0493(1967)095<0541:OTOSHI>2.3.CO;2.
- Kursinski, E. R., G. A. Hajj, J. T. Schofield, R. P. Linfield, and K. R. Hardy (1997), Observing Earth's atmosphere with radio occultation measurements using the Global Positioning System, *J. Geophys. Res.*, *102*, 23,429–23,465, doi:10.1029/97JD01569.
- Kursinski, E. R., G. A. Hajj, S. S. Leroy, and B. Herman (2000), The GPS radio occultation technique, *TAO*, *11*, 53–114.
- Landsea, C., and J. Franklin (2013a), How 'good' are the best tracks? Estimating uncertainty in the Atlantic hurricane database, *Mon. Weather Rev.*, *141*, 3576–3592, doi:10.1175/MWR-D-12-00254.1.
- Landsea, C. W., and J. L. Franklin (2013b), Atlantic hurricane database uncertainty and presentation of a new database format, *Mon. Weather Rev.*, *141*, 3576–3592, doi:10.1175/MWR-D-12-00254.1.
- Liu, H., J. Anderson, and Y.-H. Kuo (2012), Improved analyses and forecasts of Hurricane Ernesto's genesis using radio occultation data in an ensemble filter assimilation system, *Mon. Weather Rev.*, *140*, 151–166, doi:10.1175/MWR-D-1100024.1.
- Liu, Y., D.-L. Zhang, and M. K. Yau (1999), A multiscale numerical study of Hurricane Andrew (1992). Part II: Kinematics and inner-core structures, *Mon. Weather Rev.*, *127*, 2597–2616, doi:10.1175/1520-0493(1999)127<2597:AMNSOH>2.0.CO;2.
- Luo, Z., G. L. Stephens, K. A. Emanuel, D. G. Vane, N. D. Tourville, and J. M. Haynes (2008), On the use of CloudSat and MODIS data for estimating hurricane intensity, *IEEE Geosci. Remote Sens. Lett.*, *5*, 13–16, doi:10.1109/LGRS.2007.905341.

- Molinari, J., and D. Vollaro (2008), Extreme helicity and intense convective towers in Hurricane Bonnie, *Mon. Weather Rev.*, *136*, 4355–4372, doi:10.1175/2008MWR2423.1.
- Montgomery, M. T., M. E. Nicholls, T. A. Cram, and A. B. Saunders (2006), A vortical hot tower route to tropical cyclogenesis, *J. Atmos. Sci.*, *63*, 355–386, doi:10.1175/JAS3604.1.
- Murnane, R. J., and J. B. Elsner (2012), Maximum wind speeds and US hurricane losses, *Geophys. Res. Lett.*, *39*, L16707, doi:10.1029/2012GL052740.
- Papas, C. H. (1965), *Theory of Electromagnetic Wave Propagation*, McGraw Hill, New York.
- Powell, M. D., S. H. Houston, and T. A. Reinhold (1996), Hurricane Andrew's landfall in South Florida. Part I: Standardizing measurements for documentation of surface wind fields, *Weather Forecast.*, *11*, 304–328, doi:10.1175/1520-0434(1996)011<0304:HALISF>2.0.CO;2.
- Reid, G. C., and K. S. Gage (1996), The tropical tropopause over the western Pacific: Wave driving, convection, and the annual cycle, *J. Geophys. Res.*, *101*, 21,233–21,241, doi:10.1029/96JD01622.
- Riehl, H., and J. S. Malkus (1958), On the heat balance in the equatorial trough zone, *Geophysica*, *6*, 503–538.
- Riehl, H., and J. S. Simpson (1979), The heat balance of the equatorial trough zone, revisited, *Contrib. Atmos. Phys.*, *52*, 287–305.
- Rienecker, M. M., et al. (2011), MERRA: NASA's modern-era retrospective analysis for research and applications, *J. Clim.*, *24*, 3624–3648, doi:10.1175/JCLI-D-11-00015.1.
- Romps, D. M., and Z. Kuang (2009), Overshooting convection in tropical cyclones, *Geophys. Res. Lett.*, *36*, L09804, doi:10.1029/2009GL037396.
- Rozoff, C. M., W. H. Schubert, and J. P. Kossin (2008), Some dynamical aspects of tropical cyclone concentric eyewalls, *Q. J. R. Meteorol. Soc.*, *134*, 583–593, doi:10.1002/qj.237.
- Ruf, C. S., S. Gleason, Z. Jelenak, S. Katzberg, A. Ridley, R. Rose, J. Scherrer, and V. Zavorotny (2012), The CYGNSS nanosatellite constellation hurricane mission, *IEEE International Geoscience and Remote Sensing Symposium*, Munich, Germany, 22–27 July.
- Russell, L. R. (1971), Probability distributions for hurricane effects, *J. Wtrwy. Harb. Coast. Eng. Div. ASCE*, *97*(1), 139–154.
- Sampson, C. R., and A. J. Schrader (2000), The automated tropical cyclone forecasting system (Version 3.2), *Bull. Am. Meteorol. Soc.*, *81*, 1231–1240, doi:10.1175/1520-0477(2000)081<1231:TATCFS>2.3.CO;2.
- Simpson, J., J. B. Halverson, B. S. Ferrier, W. A. Petersen, R. H. Simpson, R. Blakeslee, and S. L. Durden (1998), On the role of “hot towers” in tropical cyclone formation, *Meteorol. Atmos. Phys.*, *67*, 15–35, doi:10.1007/BF01277500.
- Teshiba, M., H. Fujita, H. Hashiguchi, Y. Shibagaki, M. D. Yamanaka, and S. Fukao (2005), Detailed structure within a tropical cyclone “eye”, *Geophys. Res. Lett.*, *32*, L24805, doi:10.1029/2005GL023242.
- Thompson, E. F., and V. J. Cardone (1996), Practical modeling of hurricane surface wind fields, *J. Wtrwy. Port Coast. Ocean Eng. ASCE*, *122*(4), 195–205, doi:10.1061/(ASCE)0733-950X(1996)122:4(195).
- Velden, C., et al. (2006), The Dvorak tropical cyclone intensity estimation technique: A satellite-based method that has endured for over 30 years, *Bull. Amer. Meteor. Soc.*, *87*, 1195–1210, doi:10.1175/BAMS-87-9-1195.
- Vergados, P., A. J. Mannucci, and H. Su (2013), A validation study for GPS radio occultation data with moist thermodynamic structure of tropical cyclone, *J. Geophys. Res. Atmos.*, *118*, 9401–9413, doi:10.1002/jgrd.50698.
- Vickery, P. J., and A. Twisdale (1995), Wind-field and filling models for hurricane wind speed predictions, *J. Struct. Eng. ASCE*, *121*, 1700–1709, doi:10.1061/(ASCE)0733-9445(1995)121:11(1700).
- Vickery, P. J., P. F. Skerlj, A. C. Steckley, and L. A. Twisdale (2000), Hurricane wind field model for use in hurricane simulations, *J. Struct. Eng.*, *126*, 1203–1221, doi:10.1061/(ASCE)0733-9445(2000)126:10(1203).
- Wong, V., and K. Emanuel (2007), Use of cloud radars and radiometers for tropical cyclone intensity estimation, *Geophys. Res. Lett.*, *34*, L12811, doi:10.1029/2007GL029960.
- Yang, Y.-T., H.-C. Kuo, E. A. Hendricks, and M. S. Peng (2013), Structural and intensity changes of concentric eyewall typhoons in the Western North Pacific basin, *Mon. Weather Rev.*, *141*, 2632–2648, doi:10.1175/MWR-D-12-00251.1.
- Zhang, J. A., P. G. Black, J. R. French, and W. M. Drennan (2008), First direct measurements of enthalpy flux in the hurricane boundary layer: The CBLAST results, *Geophys. Res. Lett.*, *35*, L14813, doi:10.1029/2008GL034374.